

DOI: 10.1002/ ((please add manuscript number))

**Article type: Full Paper**

## Gas-Stabilizing Gold Nanocones for Acoustically Mediated Drug Delivery

*Christophoros Mannaris<sup>†</sup>, Boon M. Teo<sup>†</sup>, Anjali Seth, Luca Bau, Constantin Coussios<sup>\*</sup> and Eleanor Stride<sup>\*</sup>*

<sup>†\*</sup> contributed equally to the work

Dr. C. Mannaris, Dr. B. M. Teo, Dr. A. Seth, Dr. L. Bau, Prof. C. C. Coussios, Prof. E. Stride  
Institute of Biomedical Engineering, Old Road Campus Research Building, University of Oxford,  
Oxford OX3 7DQ, UK

E-mail: [eleanor.stride@eng.ox.ac.uk](mailto:eleanor.stride@eng.ox.ac.uk), [constantin.coussios@eng.ox.ac.uk](mailto:constantin.coussios@eng.ox.ac.uk)

Dr. B. M. Teo  
Interdisciplinary Nanoscience Center (iNANO), The iNANO House, Gustav Wieds Vej 14, Aarhus  
University, DK-8000 Aarhus C, Denmark

Dr. B. M. Teo  
School of Chemistry, Monash University, 19 Rainforest Walk, Clayton VIC 3800, Australia

**Keywords: ultrasound, drug delivery, cavitation, nanoparticles, extravasation**

*The efficient penetration of drugs into tumors is a major challenge that remains unmet. Reported herein is a strategy to promote extravasation and enhanced penetration using inertial cavitation initiated by focused ultrasound and cone-shaped gold nanoparticles that entrap gas nanobubbles. The cones are capable of initiating inertial cavitation under pressures and frequencies achievable with existing clinical ultrasound systems and of promoting extravasation and delivery of a model large therapeutic molecule in an in vitro tissue mimicking flow phantom, achieving penetration depths in excess of 2 mm. Ease of functionalization and intrinsic imaging capabilities provide gold with significant advantages as a material for biomedical applications. The cones do not show cytotoxicity in MCF-7 cells nor hemolytic activity in human blood at clinically relevant concentrations, and are found to be colloidally stable for at least 5 days at 37 °C and several months at 4 °C.*

## 1. Introduction

An important attribute of the tumor microenvironment is the combination of a leaky vasculature and lack of healthy lymphatics, resulting in an increase in interstitial fluid pressure. This presents a major limitation for the efficient and uniform distribution of therapeutics into the tumor, particularly macromolecular anticancer agents such as antibodies, drug-carrying nanoparticles and viral vectors, and is driving the research community into developing alternative drug delivery systems to overcome this obstacle.

Theranostic nanoplatforms hold great potential in the diagnosis and treatment of solid tumors and have become a very active area of cancer research. Nanoparticles can be used to deliver a range of diagnostic and/or therapeutic agents via chemical conjugation or physical encapsulation. Stimuli-responsive nanoscale devices sensitive to specific endogenous stimuli such as low pH<sup>[1]</sup> and hypoxia,<sup>[2]</sup> or extracorporeal physical stimuli such as light,<sup>[3–5]</sup> heat,<sup>[6,7]</sup> magnetic fields,<sup>[8]</sup> and ultrasound<sup>[9–12]</sup> have been engineered in order to improve both spatial and temporal control of drug delivery.<sup>[13]</sup>

Due to its non-invasive, non-ionizing nature and its ability to reach depths inside the body inaccessible to most extracorporeal physical stimuli, ultrasound has received considerable attention as a means of promoting drug delivery in recent years. Remote activation of small gaseous pockets by ultrasound and the resulting acoustic cavitation<sup>[14]</sup> has been used to enhance the extravasation, penetration and distribution of anticancer agents into solid tumors.<sup>[11,15]</sup> Microstreaming associated with cavitation activity<sup>[16,17]</sup> has been shown to promote the penetration and extravasation of free drugs for a variety of applications. Bubbles expand and contract in response to the negative and positive pressure phases of the ultrasound wave. Low acoustic pressure amplitudes lead to stable, low energy bubble oscillations, known as non-inertial cavitation, and the onset of nonlinear scattering characterized by narrowband emissions in the frequency domain. Such non-inertial cavitation activity has been exploited for applications ranging from sonothrombolysis to reversible

cell membrane sonoporation.<sup>[18–20]</sup> High acoustic pressure amplitudes lead to rapid expansion and violent collapse of the bubbles, a process known as inertial cavitation (IC),<sup>[21]</sup> inducing shockwaves and liquid microjets when in proximity to physical boundaries such as vessel walls or cell membranes.<sup>[22]</sup> Microstreaming associated with inertial cavitation has been shown to be most effective at transporting macromolecular therapeutics against elevated intratumoural pressure and across a dense extracellular matrix away from vasculature.<sup>[23]</sup> In addition, the broadband emissions from inertially cavitating bubbles can be monitored in real-time via active or passive acoustic mapping, thus enabling real time imaging of the drug delivery process.<sup>[24–26]</sup>

To date, the majority of the studies utilizing IC to mechanically enhance drug delivery have used micrometer sized gas bubbles.<sup>[12,27,28]</sup> One major drawback of microbubbles is that their relatively large diameter limits their circulation half-life. They also undergo rapid destruction upon ultrasound exposure.<sup>[29]</sup> Accordingly, ultrasound-assisted drug delivery with microbubbles is largely restricted to vascular targets, rather than targets that lie beyond the endothelium, and the cavitation activity required for efficient drug penetration can only be sustained for relatively short periods compared to the half-life of most therapeutics.

To overcome this issue, researchers have sought to engineer longer circulating submicron-sized particles, capable of promoting sustained cavitation activity for ultrasound enhanced drug delivery. Perfluorocarbon based nanoemulsions,<sup>[30]</sup> polymeric microcapsules, micelles and liposomes, are some interesting acoustically sensitive nanoplatforms.<sup>[31]</sup> One such platform, recently reported by our group, is a submicron polymeric cup<sup>[32,33]</sup> capable of stabilizing nano-sized gas pockets within its cavity and exhibiting IC at low acoustic intensities achievable with existing diagnostic and therapeutic systems. The gas pocket is easily introduced in their cup-shaped cavity by re-dispersing in water after drying. These polymeric nanoparticles also showed extended cavitation activity, at least four times longer than typical microbubbles, and a 10-fold increase in reporter gene expression following ultrasound-enhanced delivery of vaccinia virus with submicron cups compared to co-administration with microbubbles.<sup>[34]</sup>

Continuing along this line of research, we reasoned that a similar strategy could be exploited to use other anisotropic nanoparticles as submicron cavitation nuclei. Gold was chosen as a core material due to its biocompatibility, ease of functionalization and intrinsic imaging capabilities through, for example, surface-enhanced Raman scattering (SERS) or the photoacoustic effect. We speculated that the cone-shaped gold nanoparticles recently reported by Zhang et al. <sup>[35]</sup> could be modified to enable stabilization of gas on their surface in the same way as the submicron polymeric cups described above. We loaded the nanocones with air by drying and re-dispersing in water, and found that they can indeed act, in their gas-loaded form, as cavitation nuclei. After testing the nanocones for colloidal stability, cytotoxicity and hemolytic activity, we determined the acoustic conditions required to initiate sustained IC and demonstrated the acoustically-triggered extravasation of co-administered virus-sized latex nanoparticles in a blood vessel phantom. The extravasation process was successfully monitored in real-time via a conventional scanner using harmonic ultrasound imaging.

## 2. Results

### 2.1. Synthesis and characterization of gold nanocones

The gold nanocones were synthesized according to a published protocol <sup>[35]</sup>, but the procedure was subsequently modified to enable stabilization of gas on their surface. Briefly, they were prepared by sonication of a biphasic water/hexane mixture containing chloroauric acid and o-phenetidine as a reducing agent. Gold particles nucleated at the liquid-liquid interface of an acoustically-generated oil-in-water emulsion grow into half-shells before undergoing a shape transformation induced by collapsing bubbles of vaporized hexane. **Figure 1a,b** shows transmission electron microscopy (TEM) images of gold nanocones, demonstrating their cone-shaped structure. The gold nanocones have hollow cavities, which we hypothesized could be used to entrap gas bubbles. The distribution of hydrodynamic diameters as determined by dynamic light scattering (DLS) is centered around 200 nm (Figure 1c), in good agreement with the TEM images showing a cavity width of approximately 150

nm. A typical batch has a gold concentration of 260  $\mu\text{g/mL}$  and a particle concentration of  $1.2 \cdot 10^9$  particles/mL.

### 2.1.1. Stability of gold nanocones

The colloidal stability of nanocarriers has been shown to affect the internalization of therapeutics into tumor cells and alter their overall efficacy.<sup>[36]</sup> We monitored the colloidal stability of gold nanocones in PBS at 37 °C for 5 days. Both size and polydispersity index, as measured by DLS, remained stable for the period under investigation (**Figure 2**), and for several months when stored at 4 °C.

### 2.1.2. Haemolysis and cytotoxicity of gold nanocones

Gold nanocones were tested for hemolytic activity at different concentrations and found to cause almost negligible hemolysis in comparison to the positive control up to a concentration of  $4.7 \cdot 10^8$  particles/mL (**Figure 3**).

To further investigate the safety of gold nanocones for future clinical applications, an MTS assay was performed on MCF 7 breast cancer cells in the presence of different concentrations of gold nanocones, to measure the cytotoxic response. The results are presented in **Figure 4**. No significant decrease in cell viability was found up to a concentration of  $10^9$  particles/mL (260  $\mu\text{g/mL}$ ) compared to the control. This is also the highest concentration that was tested for acoustic response and delivery efficiency.

## 2.2 Acoustic characterization

The probability of inertial cavitation (PIC) for 0.5 and 1.6 MHz as function of peak negative acoustic pressure is shown in **Figure 5**. Results are averages of a minimum three repetitions at each setting and error bars represent one standard deviation. At 0.5 MHz a pressure amplitude between 1.6-2.0 MPa is required to nucleate a reliable cavitation activity (PIC>80%). As expected, the pressure required for reliable cavitation at 1.6 MHz was slightly higher (2.5-3.0 MPa). These pressures are higher than the pressures required with cups, most likely due to the difference in size,

but still within the capabilities of existing diagnostic and therapeutic systems. There was no significant cavitation in the absence of the gold nanocones for any of the pressures investigated. The acoustic emission signature of a bubble depends on the bubble behavior in an ultrasound field. Non-inertial cavitation, indicative of sustained volumetric bubble oscillations, tends to be characterized by narrowband frequency-domain emissions at harmonics, subharmonics and ultra-harmonics of the main excitation frequency, whereas IC is accompanied by broadband noise emissions. **Figure 6** shows representative traces (first column) received with a passive cavitation detector (PCD) and their corresponding frequency domain (second column) during ultrasound exposure at 1.6 MHz. It is immediately evident that the gold nanocones remain unresponsive at low acoustic pressures and transition to an IC regime above a certain threshold pressure. This is similar to the previously described polymeric cups<sup>[33]</sup> and contrary to microbubbles that at low pressures undergo non-inertial cavitation before transitioning to IC at the higher pressures.<sup>[37]</sup> The right column of Figure 6 shows harmonic B-mode images captured during the excitation of the gold nanocones in an agarose flow phantom at the respective pressures. The hyperechoic signal represents acoustic emissions from a bubble responding to the focused ultrasound (FUS) excitation. As the pressure increases, the proportion of gold nanocones activated by the FUS increases and covers a wider area.

### 2.3 In-vitro evaluation of drug penetration

The same tissue mimicking flow phantom setup was used to evaluate the potential of the gold nanocones as nucleation agents for cavitation enhanced drug delivery. The pore diameter of the gel vessel phantom is approximately 500 nm, which is comparable to the endothelial gap in tumor tissue.<sup>[38,39]</sup> The gold nanocone solution was co-administered with 200 nm amine-modified yellow-green fluorescent spheres (ThermoFisher, Waltham, Massachusetts, United States) **simulating delivery of a similar sized therapeutic agent like an oncolytic virus**. 1  $\mu$ L of a 20 mg/mL suspension of the model drug was added per 1 mL of solution and each solution was checked for aggregation prior to each experiment using DLS. The nanocones-model drug solution was then infused through

the flow phantom and exposed to 1.6 MHz, 3.5 MPa, 10 Hz, 5% duty cycle ultrasound.

Extravasation using other exposure conditions, as well as optimization of ultrasound parameters, are currently under investigation and are left for future communication.

Following ultrasound exposure, the flow channels were flushed with de-ionized water and a rectangular prism containing the flow channel, was excised and placed on a glass microscope slide for imaging using an inverted microscope (Eclipse Ti; Nikon Inc, USA). Side and top-view fluorescent images (excitation: 494 nm, emission: 518 nm) were acquired around each exposure location. A selection of fluorescent images following cavitation enhanced extravasation can be seen in **Figure 7**. Top-view fluorescent images of the flow channel are shown in Figure 7 (a), (b), while the corresponding side view images are shown in (d) and (e). The direction of ultrasound propagation is indicated by the arrow (bottom-to-top of page). There was no detectable extravasation when the same exposure conditions were used in the absence of gold nanocones (see Figure 7 (c) and (f)).

### 3. Discussion

The concept of gas-loading of concave nanoparticles by drying and re-dispersing in water was applied to cone-shaped gold nanoparticles with a hydrodynamic diameter of 200 nm and a cavity diameter of 150 nm. The gold nanocones were shown to be colloidal stable for at least five days in physiological conditions (at 37 °C) and for several months upon storage at 4 °C in saline, non-toxic to MCF-7 cells and non-hemolytic to human red blood cells up to a concentration of  $4.7 \cdot 10^8$  particles/mL. Most importantly, the nanocones were shown to be capable of seeding cavitation.

Analogously to previously published polymeric cups,<sup>[32]</sup> and contrary to clinically used microbubbles, gold nanocones transition from a no-response state at low pressure amplitudes, to a fully IC state above an acoustic pressure threshold, identified as 1.6 MPa at 0.5 MHz and 2.5 MPa at 1.6 MHz. These thresholds are slightly higher but comparable to those recently identified by Kwan, Graham et al. (2015) for similarly sized polymeric sub-micron cups entrapping 100 nm

nanobubbles respectively, and could be lowered further by increasing the overall particle size and entrapped nanobubble size as also demonstrated in same work.<sup>[33]</sup>

Nevertheless, the pressures required to “release” the stabilized nanobubbles from the cone cavity and nucleate IC are low enough to be achievable with existing diagnostic and therapeutic systems, which is a major advantage in terms of clinical translation. Gold nanocones also offer various advantages over other types of acoustically active agents, such as the simple one step synthesis method, less toxic chemicals required in the synthesis, ease of functionalization with other ligands and intrinsic imaging capabilities through surface-enhanced Raman scattering (SERS) or photoacoustic imaging. Our *in-vitro* haemolysis and cytotoxicity results are consistent with the results reported by Huang et al.<sup>[40]</sup>, who tested the same nanocones *in vivo* and *in vitro* in the same concentration range that we used for our experiments, and did not find any significant decrease in cell viability or obvious signs of damage or inflammation. The small size of these agents addresses one of the main limitations of current ultrasound enhanced cancer treatments, namely the inability of the larger microbubbles to extravasate from the vasculature and follow the drug into the tumor interstitial space. During the *in-vitro* extravasation experiments, gold nanocones facilitated the penetration of a large therapeutic agent into a tissue mimicking phantom at a remarkable distance of over 2 mm (Figure 7). We believe that the ability of the nanocones to extravasate passively (or actively) through the phantom pores contributes to causing more damage to the gel in subsequent cavitation events. A similar effect is expected *in-vivo* when the nanocones extravasate into the tumor interstitium during treatment and further propel the drug deeper into the tumor.

A potential additional advantage of gold nanocones is the high density of gold. As recently shown by Mo et. al.<sup>[41]</sup> and Lea-Banks, et. al.<sup>[42]</sup> denser particles exhibit significantly greater ultrasound-mediated transport than their lower density counterparts, indicating that density is a key consideration in the design of nanoscale therapeutics. A heavier cavitation seeding agent will also penetrate deeper into a tumor thus further enabling the transport of pharmaceuticals into deeper parts of the tumor. The easy functionalization of gold surfaces with a diverse array of species such



as antibodies,<sup>[43]</sup> drugs,<sup>[44]</sup> radiopharmaceuticals,<sup>[45]</sup> polymers,<sup>[46]</sup> and viruses,<sup>[47]</sup> together with some of the intrinsic properties of gold at the nanoscale, such as the photothermal effect, could thus be exploited in future work to develop the nanocones into versatile platforms for ultrasound-enhanced drug delivery, penetration and distribution to tumors.

#### 4. Conclusion

An ultrasound-activated cone shaped gold nanoparticle of mean diameter of 200 nm and capable of seeding inertial cavitation and facilitating extravasation and delivery of a large model therapeutic has been manufactured and characterized. The versatility of gold surfaces with respect to functionalization and the good biocompatibility and high colloidal stability of gold nanocones compared to other solid nanoparticles make these agents an exciting new platform for ultrasound enhanced drug delivery in oncological and other biomedical applications.

#### 5. Experimental section

##### 5.1 Materials

o-Phenetidine, gold (III) chloride hydrate (99.999%), and hexane were purchased from Sigma-Aldrich UK and used as received. Fetal bovine serum (FBS), phosphate buffered saline (PBS) and Dulbecco's Modified Eagle's Medium (DMEM) were purchased from Life Technologies Ltd (Paisley, UK). MTS assay was purchased from Promega UK, Southampton, UK. MilliQ water (18 M $\Omega$ ·cm) was used in all experiments and degassed MilliQ water in experiments involving ultrasound.

##### 5.2 Methods

###### 5.2.1 Synthesis of gold nanocones

The nanocones were synthesized according to a published procedure.<sup>[35]</sup> An aqueous solution of HAuCl<sub>4</sub> (5 mL, 0.8 mM) was pre-heated at 50°C for 5 minutes in an ultrasound bath. A solution of o-phenetidine in hexane (2.5 mL, 20 mM) was slowly added to the aqueous phase. The mixture was

sonicated for 90 minutes at 50°C. The mixture turned opaque and purple and was allowed to phase separate overnight. The aqueous phase was collected and centrifuged at 9000 g for 20 minutes three times, air dried, re-dispersed in 3 mL of water and stored at 4°C for further characterization.

### 5.2.2. Size distribution

The hydrodynamic diameter of the gold nanocones was measured by dynamic light scattering (DLS) using a Zetasizer Nano ZS (Malvern Instruments, UK). The measurements were carried out on three different batches at 20 °C and 37 °C. The size and shape of gold nanocones were determined by TEM using a FEI Tecnai 12 microscope (FEI Company, USA). A 10 µL sample of gold nanocones was deposited on a Formvar/carbon supported copper grid. The grid was dried in air for 1 hour at room temperature before observations. The concentration of gold nanocones dispersed in PBS at pH 7.4 was measured by nanoparticle tracking analysis (NTA) on a NanoSight LM-20 (NanoSight, UK).

## 5.3 Acoustic properties

The acoustic response of the gold nanocones was measured in a tissue mimicking flow phantom with an embedded 1-mm channel through which the nanocones were flowed (Figure 8). A FUS transducer (H107, Sonic Concepts, Bothell, WA, USA) of fundamental frequency 0.5 MHz was used to excite the gold nanocones, while a PCD transducer (V320 Panametrics, Olympus, Waltham, USA) was used to record any acoustic emissions as described previously.<sup>[33,48]</sup> The flow phantom was created from a degassed biocompatible hydrogel composed of 1% (w/v) low melting point ultrapure agarose gel (Invitrogen, Carlsbad, CA, USA). A picture of the flow phantom is displayed in Figure 8.

The FUS and PCD were coaxially and confocally aligned via a central circular opening in the FUS which was in-turn aligned with the middle of the agarose channel. The FUS was previously calibrated using a 0.4-mm-diameter needle hydrophone (ONDA 1056, Onda Corporation). Both

FUS and PCD are fully controlled from custom-made software using graphical programming language (LabVIEW, National Instruments, Austin, TX, USA). Experiments were carried out at two driving center frequencies, 0.5 and 1.6 MHz.

The frequency spectra of the emissions recorded by the PCD were used to determine the response of the gold nanocones to ultrasound as well as to determine the pressure threshold required to initiate cavitation activity. 200-cycle FUS excitation pulses of increasing pressure were transmitted whilst a continuous flow of nanocones passed through the phantom, allowing for complete replenishment of the exposed region between each pulse. The background and signal segments of each trace were analyzed in MATLAB (Mathworks, Natick MA, USA) to determine if IC had occurred, and the full ensemble of PCD traces were reviewed to calculate a probability of cavitation at the prescribed ultrasound settings. The identification of IC was based upon broadband spectral elevation in the signal relative to the background. For this analysis, FUS harmonic components were removed either with a comb filter or sum of harmonics<sup>[49]</sup> processing. Harmonic-suppressed traces were deemed to exhibit IC when the mean-squared signal to background ratio exceeded  $e^3$  ( $\approx 20$ )

A Zonare Z.One (Mindray, Shenzhen, China) ultrasound scanner was used to provide real-time imaging during the experiment. The imaging allowed us to monitor the integrity of the channel, detect possible leaks, and make sure the flow was uniform and without any air bubbles. Harmonic imaging was used at a low, mechanical index in order to avoid any interference of the imaging with the therapeutic pulse and the response of the nanocones.

## 5.4 Cytotoxicity

*Cell culture.* MCF 7 breast cancer cells were cultured in RPMI medium supplemented with 10% FBS and 1% penicillin-streptomycin at 37 °C in 5% CO<sub>2</sub> and 100% humidity.

*Cytotoxicity assay.* The cytotoxicity of gold nanocones was evaluated by an MTS assay (Life Technologies Ltd., UK) according to manufacturer's protocol. Cells were seeded in a 96-well plate

at a density of  $5 \times 10^4$  cells/well in medium (100  $\mu$ L) for 24 hours. The medium was replaced with fresh medium (100  $\mu$ L) containing gold nanocones at different particle concentrations (0.23 –  $1.2 \times 10^9$  particles/mL). After 24 h incubation, the cells were rinsed with PBS and treated with MTS reagent (10% in medium) for 2 h. The absorbance of the medium was measured using a plate reader (FLUOstar Omega, BMG Labtech, Germany).

### 5.5 Hemolysis assay

1 mL of blood sample was diluted with PBS (2 mL, pH 7.4) and centrifuged at 8000 rpm for 10 minutes. The supernatant was discarded. The purified red blood cells (RBC) were re-suspended in PBS (10 mL). Subsequently, a RBC suspension (200  $\mu$ L) was incubated with various concentrations of gold nanocones at room temperature for 3 hours under gentle shaking. PBS and water (800  $\mu$ L) were used as negative and positive control, respectively. The samples were then centrifuged at 12000 rpm for 5 minutes and the absorbance of the supernatants was measured at 540 nm.

### 5.6 Statistical Analysis

Kaleidagraph software was used for all statistical analysis. All data were averaged with error bars representing the standard deviation of  $n = 3$  runs.

The statistical significance (P value) used to compare the distribution of samples was determined using a 1-way ANOVA with a confidence level of 95% ( $\alpha = 0.05$ ), followed by a Tukey's multiple comparison post-hoc test. For the experiments with cell viability and haemolysis data (Figures 3 and 4), statistical analysis was performed using raw data, non-normalized data.

### Disclaimer

Informed signed consent was obtained from the donor for the hemolysis study.

### Acknowledgements

The authors thank the funding through the Oxford Centre for Drug Delivery Devices under programme grant EP/L024012/1 by the UK's Engineering and Physical Sciences Research Council. BMT acknowledges the Danish Council for Independent Research, Technology and Production Sciences and Sapere Aude level 1 grant. Supporting data are available through the University of Oxford ORA data repository (doi:

C. Mannaris and B. Teo contributed equally to this work

Received: ((will be filled in by the editorial staff))

Revised: ((will be filled in by the editorial staff))

Published online: ((will be filled in by the editorial staff))

## References

- [1] M. Karimi, M. Eslami, P. Sahandi-Zangabad, F. Mirab, N. Farajisafiloo, Z. Shafaei, D. Ghosh, M. Bozorgomid, F. Dashkhaneh, M. R. Hamblin, *Wiley Interdiscip. Rev. Nanomedicine Nanobiotechnology* **2016**, 8, 696.
- [2] A. Houman, S. M. Siddharth, B. G. Allan, I. G. Gregory, G. Khaled, *Curr. Pharm. Des.* **2016**, 22, 2808.
- [3] Y. Chen, H. Li, Y. Deng, H. Sun, X. Ke, T. Ci, *Acta Biomater.* **2017**, 51, 374.
- [4] A. L. Chin, Y. Zhong, R. Tong, *Biomater. Sci.* **2017**, DOI 10.1039/C7BM00348J.
- [5] T. Lajunen, L.-S. Kontturi, L. Viitala, M. Manna, O. Cramariuc, T. Róg, A. Bunker, T. Laaksonen, T. Viitala, L. Murtomäki, et al., *Mol. Pharm.* **2016**, 13, 2095.
- [6] C. S. S. R. Kumar, F. Mohammad, *Adv. Drug Deliv. Rev.* **2011**, 63, 789.
- [7] D. Needham, G. Anyarambhatla, G. Kong, M. W. Dewhirst, *Cancer Res* **2000**, 60, 1197.
- [8] S. C. McBain, H. H. P. Yiu, J. Dobson, *Int. J. Nanomedicine* **2008**, 3, 169.
- [9] P. J. Kempen, S. Greasley, K. A. Parker, J. L. Campbell, H. Y. Chang, J. R. Jones, R. Sinclair, S. S. Gambhir, J. V. Jokerst, *Theranostics* **2015**, 5, 631.
- [10] F. Foroutan, J. V Jokerst, S. S. Gambhir, O. Vermesh, H.-W. Kim, J. C. Knowles, *ACS Nano* **2015**, 9, 1868.
- [11] M. Bazan-Peregrino, B. Rifai, R. C. Carlisle, J. Choi, C. D. Arvanitis, L. W. Seymour, C. C. Coussios, *J Control Release* **2013**, 169, 40.
- [12] J. M. Escoffre, C. Mannaris, B. Geers, A. Novell, I. Lentacker, M. Averkiou, A. Bouakaz, *IEEE Trans Ultrason Ferroelectr Freq Control* **2013**, 60, 78.
- [13] S. Mura, J. Nicolas, P. Couvreur, *Nat Mater* **2013**, 12, 991.
- [14] C. C. Coussios, R. A. Roy, *Annu. Rev. Fluid Mech.* **2008**, 40, 395.
- [15] R. Carlisle, J. Choi, M. Bazan-Peregrino, R. Laga, V. Subr, L. Kostka, K. Ulbrich, C. C. Coussios, L. W. Seymour, *J Natl Cancer Inst* **2013**, 105, 1701.
- [16] R. K. Gould, *J. Acoust. Soc. Am.* **1974**, 56, 1740.

- [17] A. I. Eller, *J. Acoust. Soc. Am.* **1969**, *46*, 1246.
- [18] S. Datta, C. C. Coussios, L. E. McAdory, J. Tan, T. Porter, G. De Courten-Myers, C. K. Holland, *Ultrasound Med Biol* **2006**, *32*, 1257.
- [19] Y. Hu, J. M. Wan, A. C. Yu, *Ultrasound Med Biol* **2013**, *39*, 2393.
- [20] K. Kooiman, M. Emmer, M. Foppen-Harteveld, A. van Wamel, N. de Jong, *IEEE Trans Biomed Eng* **2010**, *57*, 29.
- [21] C. K. Holland, R. E. Apfel, *J. Acoust. Soc. Am.* **1990**, *88*, 2059.
- [22] S. Mitragotri, *Nat Rev Drug Discov* **2005**, *4*, 255.
- [23] M. Bazan-Peregrino, C. D. Arvanitis, B. Rifai, L. W. Seymour, C. C. Coussios, *J Control Release* **2012**, *157*, 235.
- [24] C. D. Arvanitis, M. S. Livingstone, N. McDannold, *Phys Med Biol* **2013**, *58*, 4749.
- [25] J. J. Choi, R. C. Carlisle, C. Coviello, L. Seymour, C. C. Coussios, *Phys Med Biol* **2014**, *59*, 4861.
- [26] K. J. Haworth, J. L. Raymond, K. Radhakrishnan, M. R. Moody, S. L. Huang, T. Peng, H. Shekhar, M. E. Klegerman, H. Kim, D. D. McPherson, et al., *Ultrasound Med Biol* **2016**, *42*, 518.
- [27] W. S. Chen, T. J. Matula, A. A. Brayman, L. A. Crum, *J. Acoust. Soc. Am.* **2003**, *113*, 643.
- [28] E. Stride, C. Porter, A. G. Prieto, Q. Pankhurst, *Ultrasound Med Biol* **2009**, *35*, 861.
- [29] C. Mannaris, M. A. Averkiou, *Ultrasound Med Biol* **2012**, *38*, 681.
- [30] K. Wilson, K. Homan, S. Emelianov, *Nat. Commun.* **2012**, *3*, DOI 10.1038/ncomms1627.
- [31] T. Boissenot, A. Bordat, E. Fattal, N. Tsapis, *J Control Release* **2016**, *241*, 144.
- [32] J. J. Kwan, S. Graham, R. Myers, R. Carlisle, E. Stride, C. C. Coussios, *Phys Rev E Stat Nonlin Soft Matter Phys* **2015**, *92*, 23019.
- [33] J. J. Kwan, R. Myers, C. M. Coviello, S. M. Graham, A. R. Shah, E. Stride, R. C. Carlisle, C. C. Coussios, *Small* **2015**, *11*, 5305.
- [34] R. Myers, C. Coviello, P. Erbs, J. Foloppe, C. Rowe, J. Kwan, C. Crake, S. Finn, E. Jackson,

J. M. Balloul, et al., *Mol Ther* **2016**, *24*, 1627.

- [35] P. Zhang, J. He, X. Ma, J. Gong, Z. Nie, *Chem. Commun.* **2013**, *49*, 987.
- [36] I. Abanades Lazaro, S. Haddad, S. Sacca, C. Orellana-Tavra, D. Fairen-Jimenez, R. S. Forgan, *Chem* **2017**, *2*, 561.
- [37] C. D. Arvanitis, M. Bazan-Peregrino, B. Rifai, L. W. Seymour, C. C. Coussios, *Ultrasound Med Biol* **2011**, *37*, 1838.
- [38] S. K. Hobbs, W. L. Monsky, F. Yuan, W. G. Roberts, L. Griffith, V. P. Torchilin, R. K. Jain, *Proc Natl Acad Sci U S A* **1998**, *95*, 4607.
- [39] M. Maaloum, N. Pernodet, B. Tinland, *Electrophoresis* **1998**, *19*, 1606.
- [40] P. Huang, P. Rong, J. Lin, W. Li, X. Yan, M. G. Zhang, L. Nie, G. Niu, J. Lu, W. Wang, et al., *J. Am. Chem. Soc.* **2014**, *136*, 8307.
- [41] S. Mo, R. Carlisle, R. Laga, R. Myers, S. Graham, R. Cawood, K. Ulbrich, L. Seymour, C. C. Coussios, *J Control Release* **2015**, *210*, 10.
- [42] H. Lea-Banks, B. Teo, E. Stride, C. C. Coussios, *Phys Med Biol* **2016**, *61*, 7906.
- [43] S. Kumar, J. Aaron, K. Sokolov, *Nat. Protoc.* **2008**, *3*, 314.
- [44] G. F. Paciotti, J. Zhao, S. Cao, P. J. Brodie, L. Tamarkin, M. Huhta, L. D. Myer, J. Friedman, D. G. I. Kingston, *Bioconjug. Chem.* **2016**, *27*, 2646.
- [45] S. Yook, Z. Cai, Y. Lu, M. A. Winnik, J. P. Pignol, R. M. Reilly, *Mol. Pharm.* **2015**, *12*, 3963.
- [46] M. S. Yavuz, Y. Cheng, J. Chen, C. M. Cobley, Q. Zhang, M. Rycenga, J. Xie, C. Kim, K. H. Song, A. G. Schwartz, et al., *Nat. Mater.* **2009**, *8*, 935.
- [47] M. Everts, V. Saini, J. L. Leddon, R. J. Kok, M. Stoff-Khalili, M. A. Preuss, C. L. Millican, G. Perkins, J. M. Brown, H. Bagaria, et al., *Nano Lett.* **2006**, *6*, 587.
- [48] N. Hockham, C. C. Coussios, M. Arora, *IEEE Trans Ultrason Ferroelectr Freq Control* **2010**, *57*, 2685.
- [49] E. Lyka, C. Coviello, R. Kozick, C. C. Coussios, *J. Acoust. Soc. Am.* **2016**, *140*, 741.



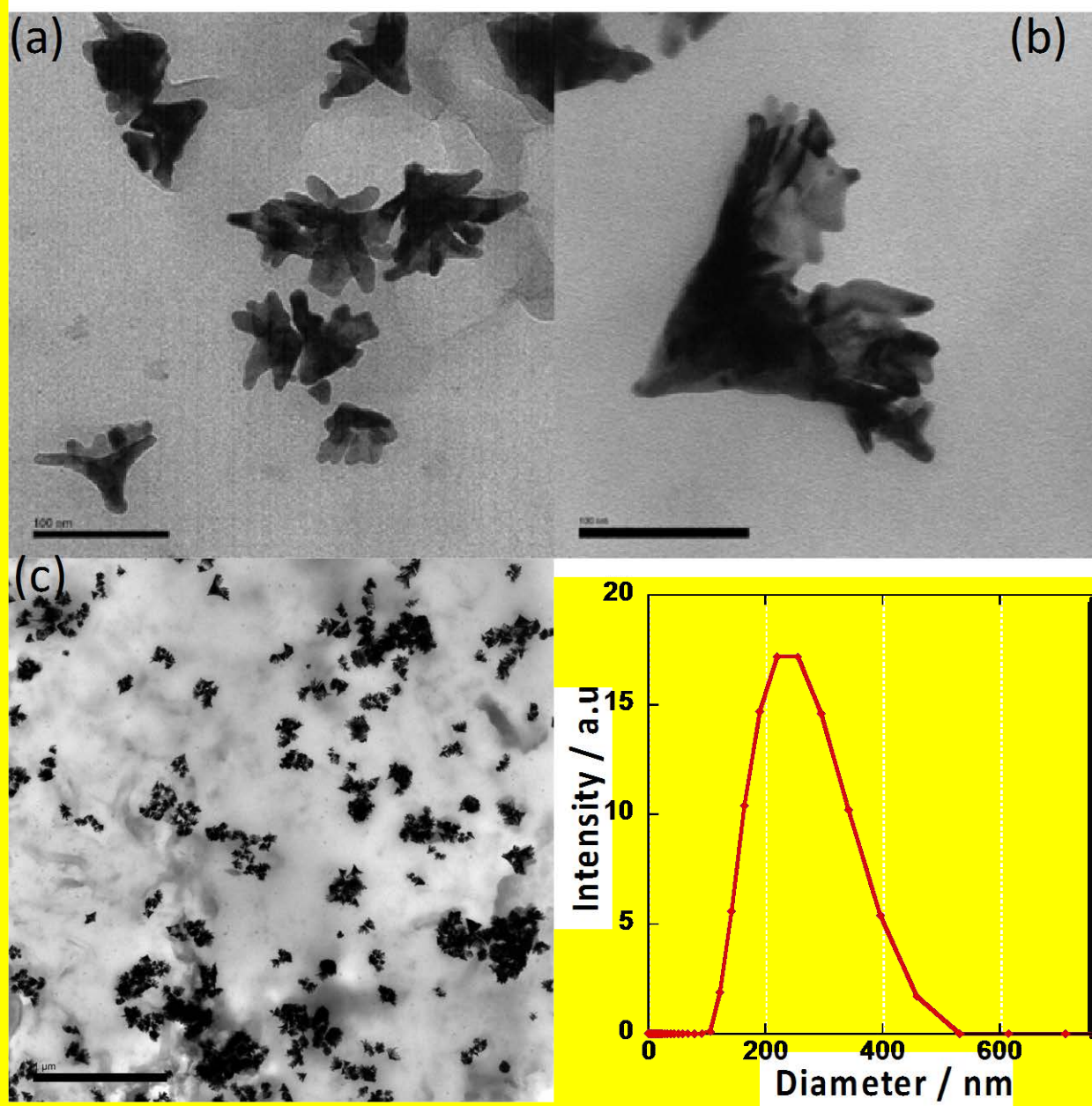


**Figure 1.** a, b, c TEM images of gold nanocones (scale bars: 100, 100, 1000 nm) and d) hydrodynamic diameter of gold nanocones.

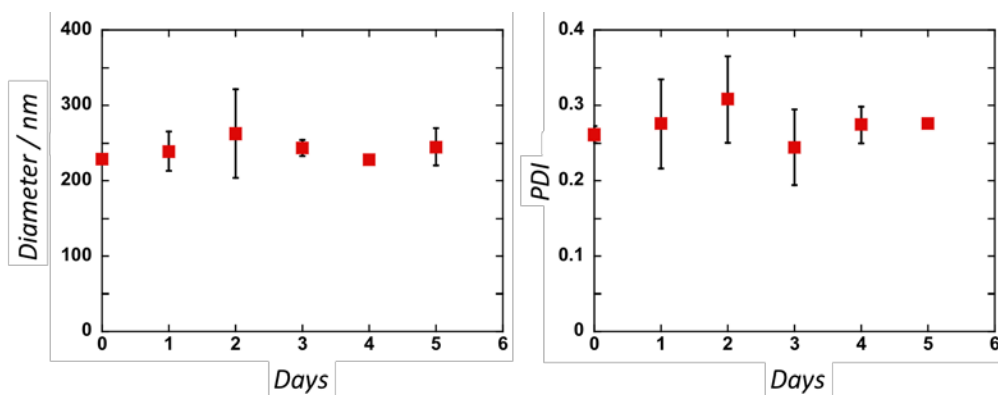


**Figure 2.** a) particle size and b) polydispersity index of gold nanocones. Data are averaged with error bars representing the standard deviation of  $n = 3$  runs.

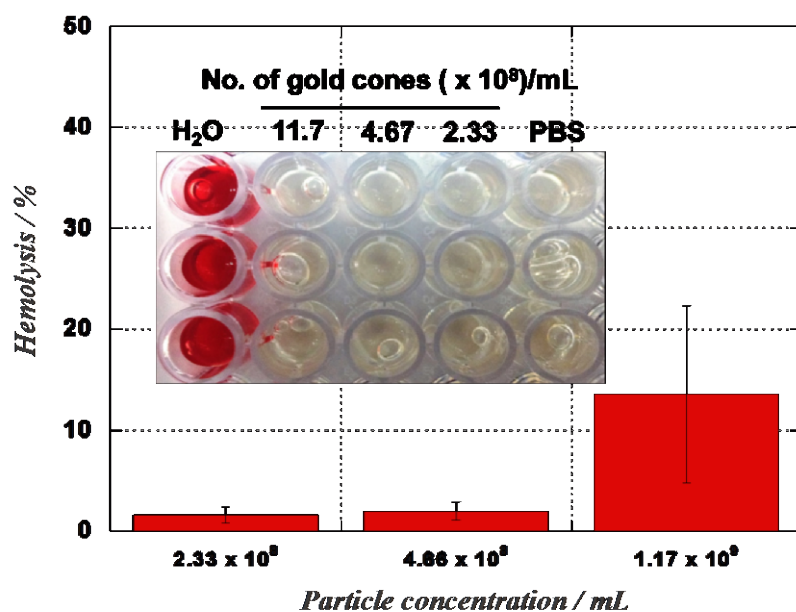


**Figure 3.** Hemolysis assay on gold nanocones following incubation of red blood cells with increasing concentrations of gold nanocones. Hemolysis levels are normalized to the positive control. Data are averaged with error bars representing the standard deviation of  $n = 3$  runs.

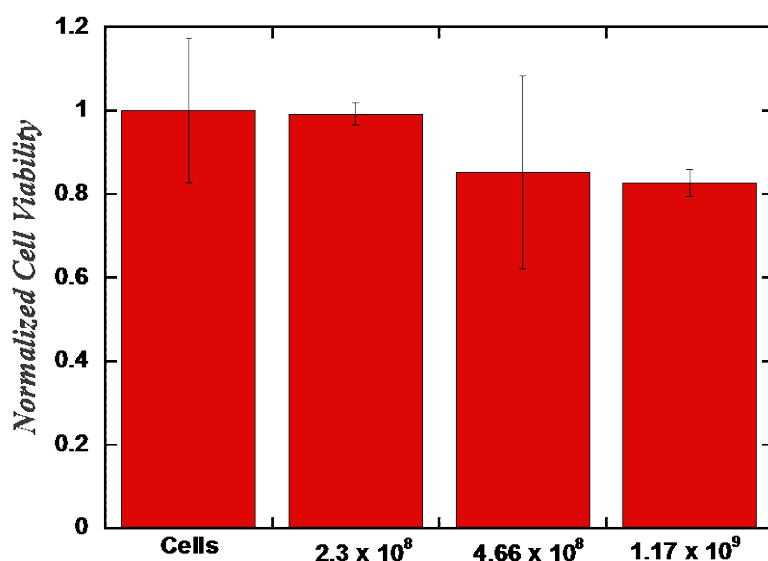


**Figure 4.** Cell viability of gold nanocones at different concentrations against MCF-7 breast cancer cells, normalized to the negative control. Data are averaged with error bars representing the standard deviation of  $n = 3$  runs.

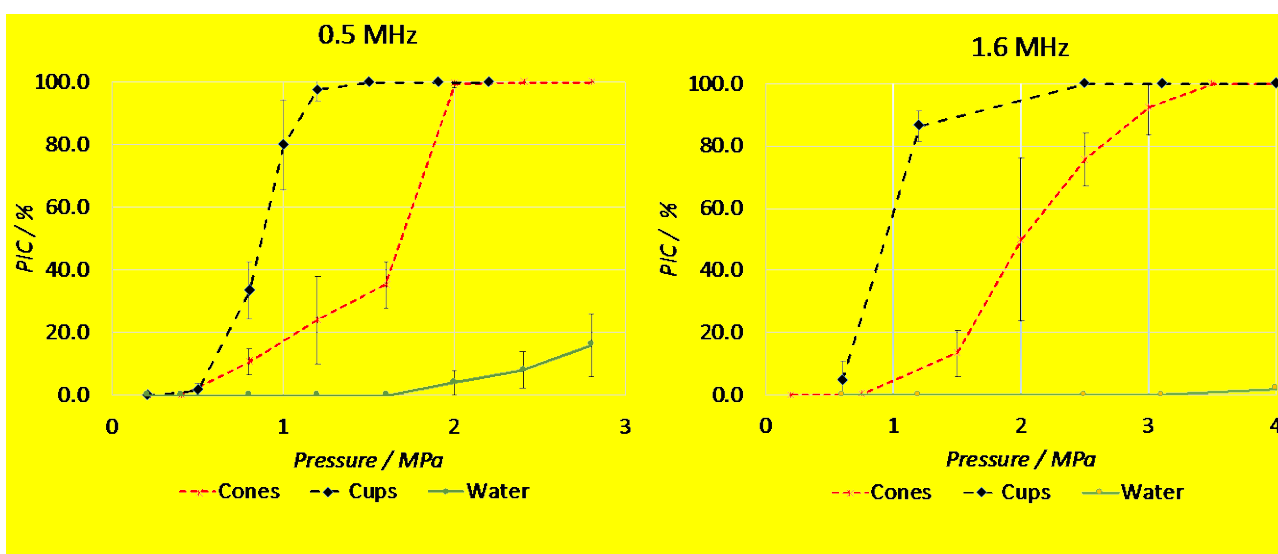


**Figure 5.** Probability of Inertial Cavitation as a function of peak negative acoustic pressure in water with and without gold nanocones or polymeric nanocups. Pressure amplitude for reliable cavitation activity is 1.5-2 MPa for 0.5 MHz (left) and 2.5-3.0 MPa for 1.6 MHz (right). Results are shown as averages of a minimum three repetitions at each setting and error bars represent one standard deviation.

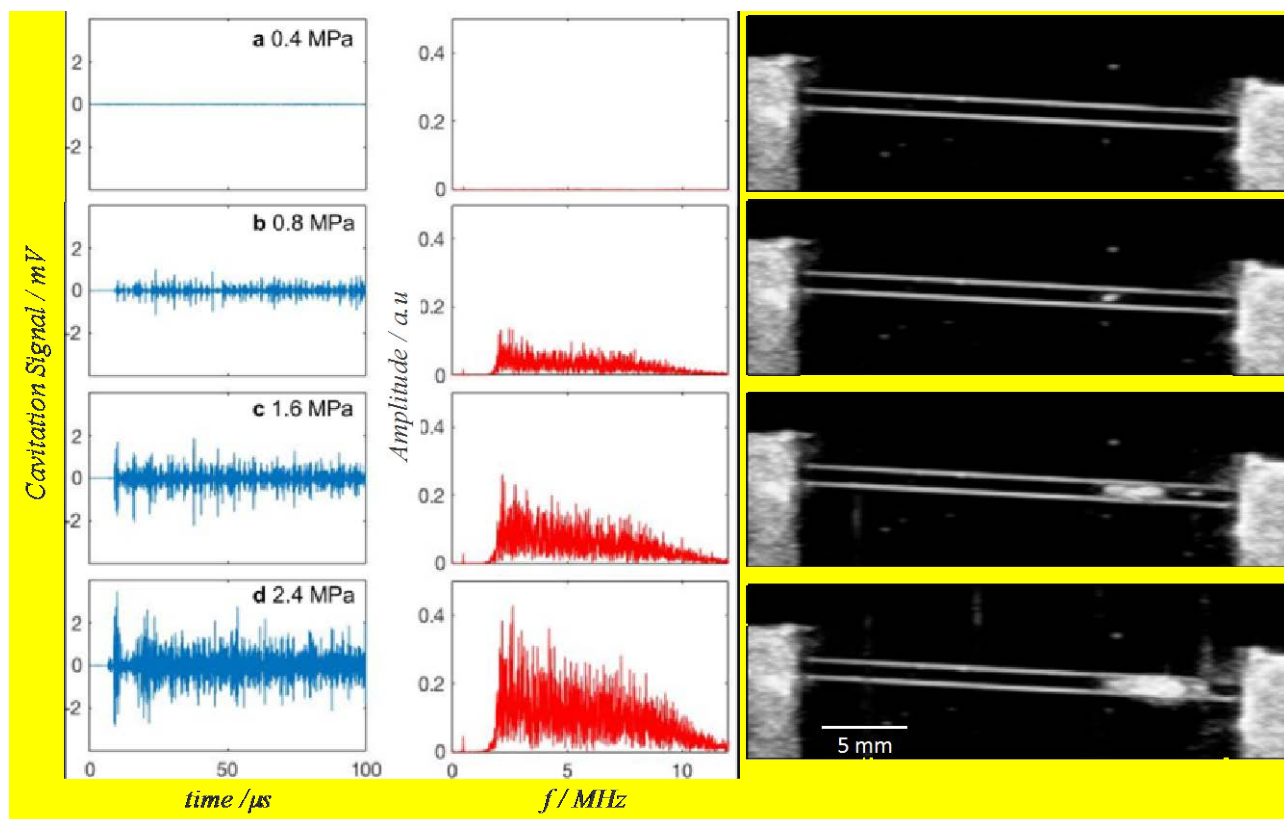


**Figure 6.** PCD time traces for varying pressures (left column) and their corresponding frequency domains (middle column). Amplitude of received signal increases with increasing pressure while broadband emissions, indicative of IC, are detected. On the right, corresponding harmonic B-Mode images of the flow channel during FUS exposure taken with an L12-5 linear probe (8.5 MHz center frequency).

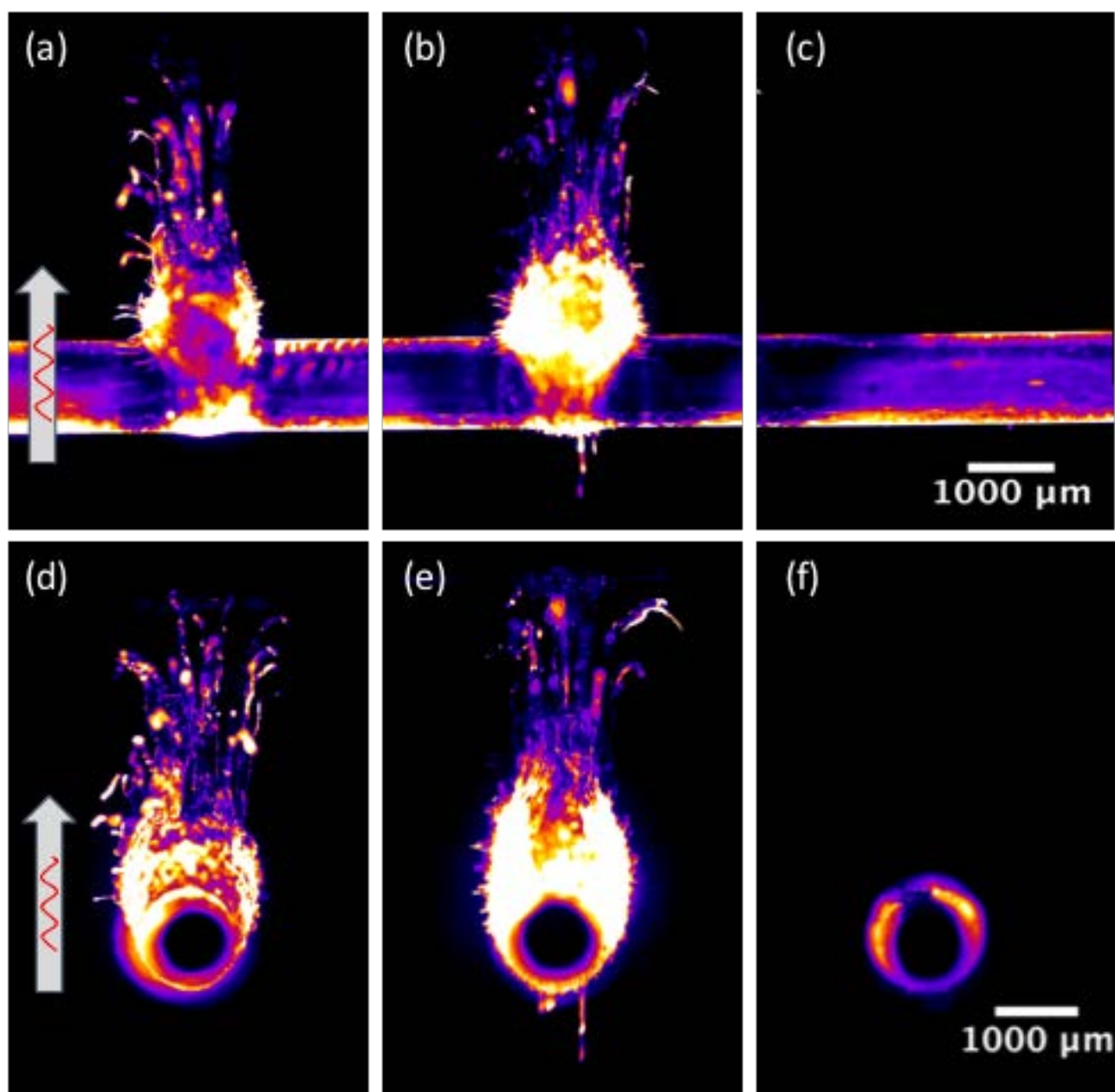


**Figure 7.** Representative fluorescent images of agarose flow channel following cavitation mediated extravasation with gold nanocones at 1.6 MHz, 3.5 MPa, 10Hz, 5% duty cycle. Top view images of agarose channel at (a) 30s exposure, (b) 60s exposure, (c) control 60s exposure without nanocones and corresponding side view images at (d-f). Direction of ultrasound propagation indicated by arrow. Deep directional extravasation observed.

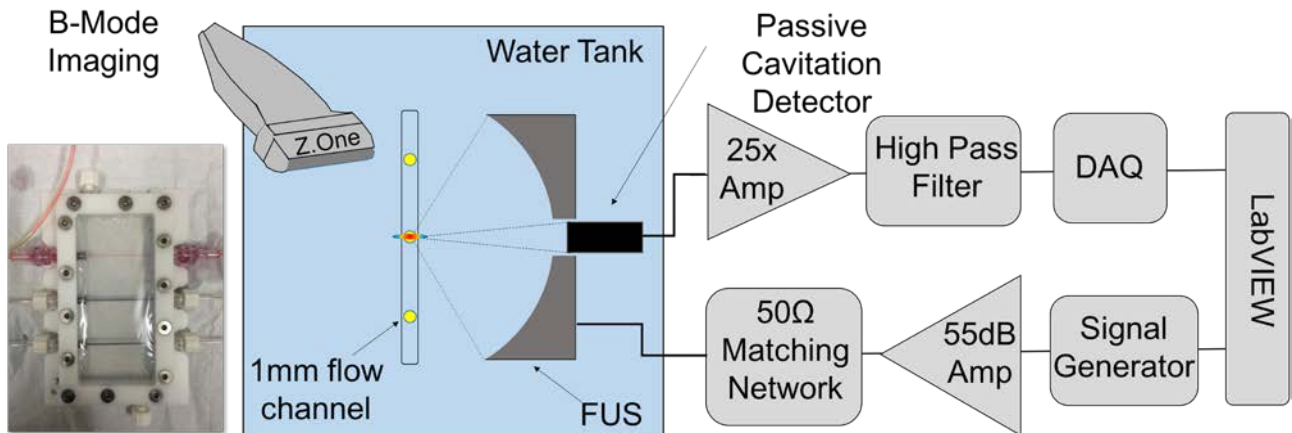


**Figure 8.** Schematic diagram of the experimental setup, illustrating the FUS generation and passive cavitation detection loop. On the left, a picture of the flow-through tissue-mimicking phantom.